






Magnetic field vector detection at the millitesla level using a YIG microcavity optical sensor

YANRAN WU,^{1,2,†} YONGPAN GAO,^{1,3,†}  YISU YANG,^{1,3,5} SONGYI LIU,^{1,2} TINGYANG PAN,^{1,2} BING DUAN,^{1,2} BINGRUI GUO,^{1,3} BOLUN ZHANG,⁴ DAQUAN YANG,^{1,2,6}  AND HUIPING TIAN^{1,2,7} 

¹State Key Laboratory of Information Photonics and Optical Communications, Beijing University of Posts and Telecommunications, Beijing 100876, China

²School of Information and Communication Engineering, Beijing University of Posts and Telecommunications, Beijing 100876, China

³School of Electronic Engineering, Beijing University of Posts and Telecommunications, Beijing 100876, China

⁴International School, Beijing University of Posts and Telecommunications, Beijing 100876, China

⁵yangyisu@bupt.edu.cn

⁶ydq@bupt.edu.cn

⁷hptian@bupt.edu.cn

[†]These authors contributed equally to this paper

Abstract: Millitesla-level magnetic field vector detection based on a yttrium iron garnet (YIG) microcavity optical sensor with a quality factor of $\sim 10^5$ is proposed and demonstrated. The sensor leverages external magnetic field variations to change the dielectric constant of the material, thereby achieving refractive index sensing. The spectrum of YIG microcavities with different crystal orientations exhibits redshift with increasing magnetic field strength, reaching a maximum intensity sensitivity of approximately 0.357 pm/mT and a saturation magnetic field strength of around 45 mT. Additionally, the sensor enables 360° magnetic field direction rotation detection, with a maximum directional sensitivity of 0.132 pm/rad. The optical sensor has a small footprint, a simple structure, and a wide measurement range.

© 2025 Optica Publishing Group under the terms of the [Optica Open Access Publishing Agreement](#)

1. Introduction

Magnetic sensors are widely used in aerospace, medical diagnostics, geological exploration, and other fields [1–6]. Traditional magnetic sensors operate based on electromagnetic induction [7–10]. However, strong magnetic field instruments are often accompanied by strong electric fields, which may degrade the sensing performance. To address these challenges, novel approaches and electric-field-insensitive materials are needed to enhance magnetic sensing capabilities. In recent years, whispering-gallery-mode (WGM) optical microresonators have emerged as crucial components in modern optics, offering promising properties such as high-quality (Q) factors and small mode volumes to enhance light-matter interactions. These properties have made WGM microresonators attractive for various sensing applications, including magnetic sensing [11–20].

WGM microcavity-based magnetic sensors have been developed as an effective solution [21–26]. However, most WGM magnetic sensors are composite microcavities formed by combining magnetic materials with WGM microcavities [27–30]. For instance, Liu et al. proposed a magnetic sensor using a microbubble cavity filled with magnetic fluid [27]. Yu et al. developed a capillary microcavity magnetic sensor filled with magnetic fluid or magnetostrictive material direct current (DC) magnetic field detection [28,29]. However, composite microcavities typically require complex nanofabrication techniques. In contrast, a new type of microcavity made of magneto-optical crystal, offering a simple magnetic sensor structure that is easier to

implement reducing manufacturing complexity and structural difficulty. Due to advantages such as shallow magnetic loss, YIG has been widely used in magnetic sensing [31–33].

In this work, we utilize a magneto-optical crystal to detect steady-state magnetic fields, achieving a magnetic field vector sensor based on YIG microsphere cavities with a Q factor of approximately 10^5 . In the experiment, two static magnets were placed side by side, and the YIG microsphere cavity positioned midway between them, where the magnetic field lines were parallel. The spectra of YIG microsphere cavities with different crystallographic orientations show a red shift as the external magnetic field strength increases. The maximum sensitivity to magnetic field strength is 0.357 pm/mT, reaching a saturation point at around 45 mT. Furthermore, the sensor can detect the direction of the magnetic field across 360° with a maximum sensitivity of 0.132 pm/rad. This magnetic field vector sensor offers a compact footprint, a simple structure, and a wide measurement range. It employs all-optical technology to achieve millitesla-level measurement, making it particularly suitable for complex electromagnetic environments and providing an efficient, safe, and reliable solution for magnetic field sensing.

2. Math and equation

When the external magnetic field changes, the refractive index of the YIG optical resonator also changes due to the opto-magnetic effect, thereby shifting the resonance wavelength of the resonator.

The resonance shift based on the magneto-optical effect in the cylindrical coordinate system is [34]:

$$G = \frac{f\epsilon_0}{2} \int dx^3 [(iu_{jr}u_{j\theta}^*M_z - iu_{jz}^*u_{jr}M_\theta + iu_{j\theta}u_{jz}^*M_r) + h.c.], \quad (1)$$

where: $f = \frac{2\sqrt{\epsilon_r}\theta_r}{k_0M_s}$, ϵ_r is the relative permittivity, θ_r is the faraday rotation coefficient, k_0 is the wave number, M_s is the saturation magnetization; ϵ_0 is the vacuum permittivity, u is the light field mode, M_r , M_z , and M_θ denote the magnetization components along the r , z , and θ directions in the cylindrical coordinate system, respectively. $h.c.$ is the Hermitian conjugate of the previous term, and $x \in \{r, \theta, z\}$. Since the sensing direction of light is perpendicular to the direction of the magnetic field, only the magnetization component M_z responds. This corresponds to the first term in the integral of the formula, which is determined by the optical mode and the magnetization component M_z . Since M_z is considered a constant, optimizing the optical mode is key to improving sensing sensitivity. When the applied magnetic field strength is within the linear region of M_z magnetization, the sensing sensitivity exhibits a good linear relationship with the frequency shift of the optical mode. Additionally, in the YIG microsphere cavity, the magnetism is only related to spin, and the frequency shift is calculated using the perturbation formula, which is independent of lattice characteristics.

3. Results and discussion

In the experiment, magneto-optical interaction was characterized by measuring the optical resonance spectra under different external magnetic field. As shown in Fig. 1(a), the diameter of the YIG microsphere cavity is 500 μm . The lasing light was coupled in and out of the microcavity through a tapered fiber that had a diameter of about 4 μm . The crystallographic orientation of the YIG microsphere resonant cavity in the experiment includes random direction, (110) direction, and (111) direction. Therefore, we are able to analyze the relationship between YIG crystal orientation and the performance of the magnetic field sensor. The coupling position between the YIG microsphere cavity and the tapered fiber was precisely controlled using a three-dimensional displacement platform, monitored by a CCD camera. Coupling was achieved via a momentum-matched evanescent field, enabling efficient excitation and precise regulation of the whispering-gallery mode. To ensure stability, both the YIG microsphere cavity and tapered

fiber were transferred to separate glass slides before coupling. Subsequently, overcoupling was used to improve coupling stability. Ultraviolet glue was applied to fix the positions of the sensing devices, achieving a semi-packaged structure to further reinforce coupling stability. This packaging method not only ensures efficient and stable coupling performance but also effectively alleviates environmental contamination.

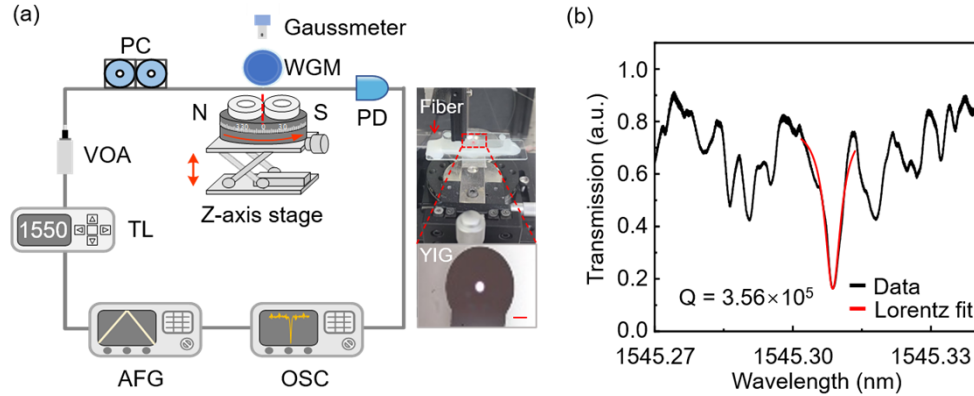


Fig. 1. (a) Schematic diagram of YIG microsphere cavity magnetic field vector sensing experimental device (left panel), TL, tunable laser; PD, photodetector; AFG, arbitrary function generator; PC, polarization controller; OSC, oscilloscope; VOA, variable optical attenuator; Physical image and optical microscope image of YIG microsphere cavity (right panel), scale bar: 100 μm . (b) Typical transmission spectrum of resonance modes of YIG microsphere cavity with (110) crystal orientation.

In the experiment, two NdFeB permanent magnets (50 mm \times 10 mm) were placed side by side on a rotating and lifting z-axis stage. The YIG microsphere cavity was positioned at the middle gap between the magnets, where magnetic field lines are parallel. This ingenious design ensures both a strong magnetic field intensity and effectively avoids temperature noise caused by the use of electromagnets [35]. The magnetic field direction can be continuously tuned from 0° to 360° by rotating the stage. A Gaussmeter monitors the magnetic field strength above the YIG microsphere cavity in real-time. In addition, the linewidth of the YIG microcavity is related to surface roughness, which depends on surface contamination and structural defects. To remove surface attachments, ultrasonic cleaning is performed. The Q factors of YIG microsphere cavities were measured to be on the order of 10^5 . Figure 1(b) shows that the Q factor of the YIG microsphere cavity magnetic sensor at (110) orientation, which is about 3.56×10^5 .

To assess the performance of the sensor, the stability of the YIG microsphere cavity was first characterized. As shown in Fig. 2(a), the shift of the resonant wavelength at room temperature was monitored in real-time. The results showed that the resonant wavelength remained stable within 5 minutes and the wavelength fluctuation variance is ~ 0.036 pm. The optical response of the microsphere cavity to the external magnetic field strength is shown in Fig. 2(b). As the magnetic field intensity increases from 10 mT to 70 mT, the resonant wavelength is redshifted from 1553.4784 nm to 1553.4818 nm. This process is also reversible.

The reversible response proves that the YIG microcavity has good reversibility of magnetic field strength. In addition, the magnetic field direction sensing capability of the YIG microsphere cavity was measured by tracking changes of the single-mode resonant wavelength under different rotation angles of the stage. The real-time response of the resonance wavelength to the magnetic field orientation angle is shown in Fig. 2(c). When the magnetic field direction was changed back to the initial value after rotating 30°/45°, the resonant wavelength also went back close to the initial value. The small uncertainty of the measurement is due to the manual operation of the

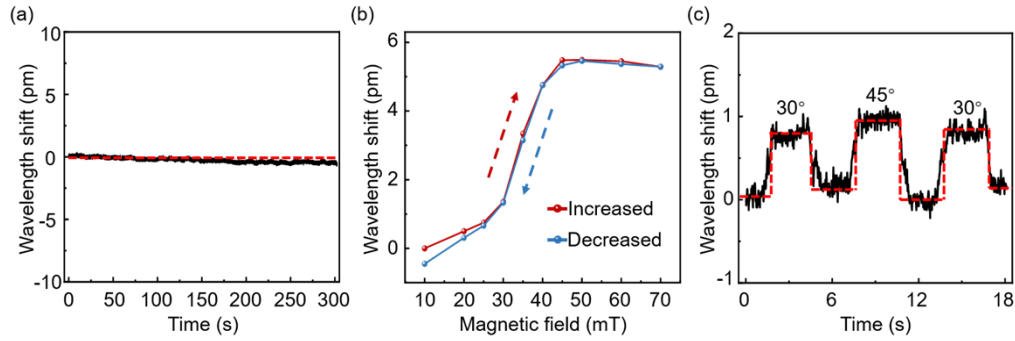


Fig. 2. (a) The long-time stability of YIG microcavity at room temperature. (b) Magnetic field strength response of YIG microcavity. Resonant wavelength experiences a red shift (red line) when magnetic field strength is increased from 10 mT to 70 mT, and a blue shift (blue line) when magnetic field strength is decreased from 70 mT to 10 mT. (c) Real-time wavelength shifts with progressively increasing and decreasing magnetic field direction.

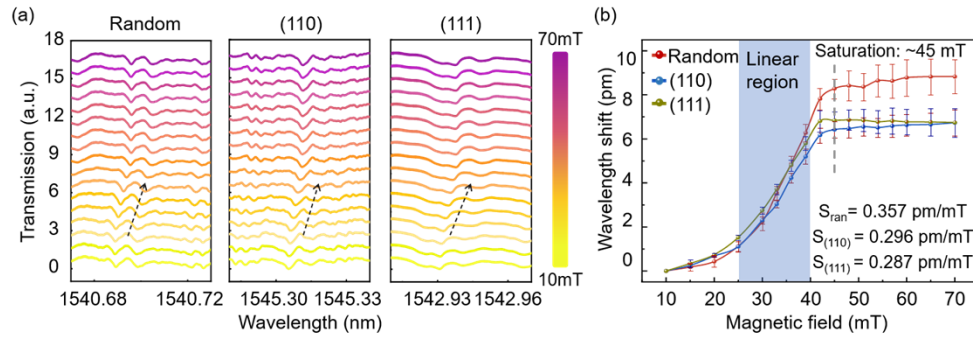


Fig. 3. (a) Transmission spectra of YIG microsphere resonators with different crystal orientations (random direction; (110); (111)) as the magnetic field strength increases from 10 mT to 70 mT. (b) Relationship between magnetic field strength and wavelength shift; data set in the blue-shaded region is used to extract the sensitivity by linear fitting. The gray dashed line represents the saturation magnetic field strength.

rotation stage. This indicates a good reversibility of the YIG microcavity to the magnetic field direction.

Figure 3(a) shows the transmission spectra of YIG microsphere cavities at different crystal orientations as a function of the external magnetic field strength that was tuned from 10 mT to 70 mT. The black dotted arrows denote tracked sensing modes, which are sufficiently separated from other modes to avoid crosstalk. Figure 3(b) demonstrates the relationship between resonant wavelength shift and magnetic field strength. The transmission spectra exhibit a redshift with an increased magnetic field before reaching the saturation threshold at around 45 mT. And there is a linear relationship between the resonant wavelength and the magnetic field strength before saturation. Notably, the fitting results reveal differences in sensitivity among the three YIG microsphere cavities with distinct crystal orientations. As analyzed theoretically in Sec. 2, crystal orientation does not influence sensitivity, which is solely determined by the optical mode. In the experiments, three YIG microsphere cavities with different crystal orientations were used. Although their shapes and dimensions are nominally identical, minor manufacturing variations prevent complete consistency. Consequently, different YIG microsphere cavities excite distinct optical modes, resulting in observed sensitivity variations. A linear fit of the experimental data

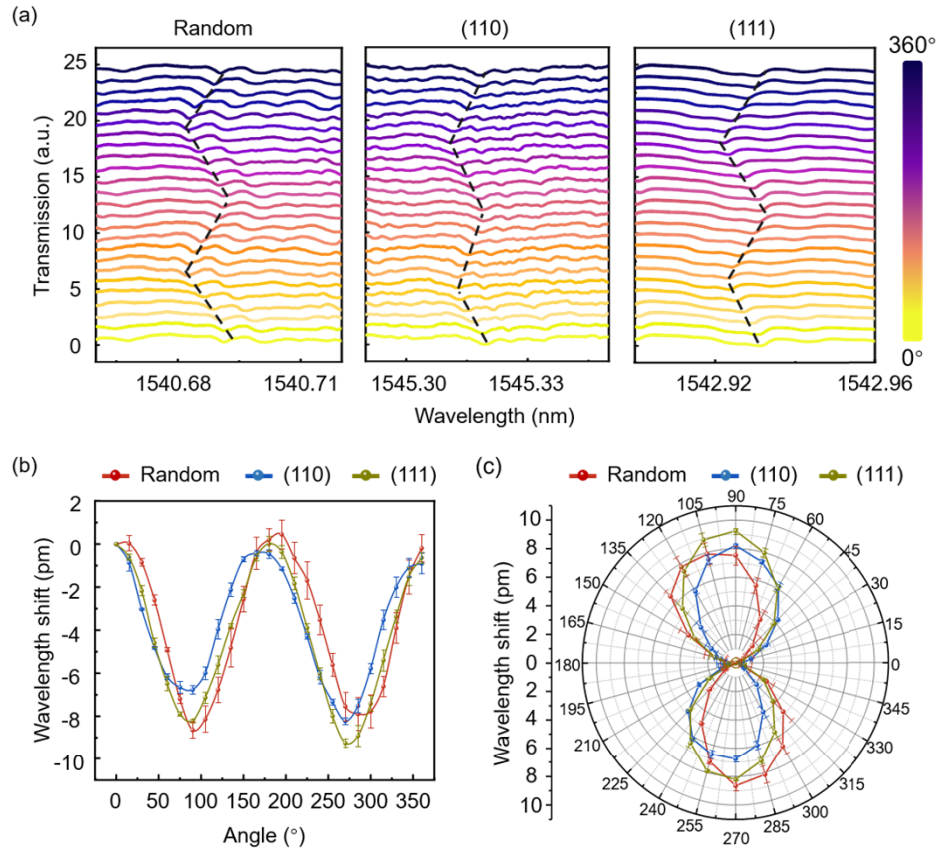


Fig. 4. (a) Transmission spectra of YIG microsphere resonators with different crystallographic orientations as the magnetic field direction changes from 0° to 360° in steps of 15° . (b) The correlation between the direction of the magnetic field and wavelength shift. (c) The wavelength varied periodically with the magnetic field angle.

in the shaded area yields a maximum strength sensitivity of 0.357 pm/mT in random direction. In addition, as shown in Fig. 2(a), the short-time noise of the resonance wavelength of the YIG cavity (the standard deviation of the 1s internal resonance wavelength shift) is about 0.07 pm . Combined with sensing sensitivity, the detection limit of the YIG magnetic field sensor is about 0.196 mT .

The direction is also a significant parameter for the magnetic field sensing applications. The transmission spectra of the YIG microsphere cavities with different crystallographic orientations as a function of the external magnetic field direction angle were measured as shown in Fig. 4(a). We tuned the magnetic field direction angle from 0° to 360° at a step of 15° while keeping the magnetic field strength at 40 mT . The black dotted lines indicate the tracked sensing modes. The shift of the resonant wavelength of the microsphere cavities is dependent on the direction of the external magnetic field. In the measurement, the magnetic field angle $0^\circ/90^\circ$ is defined in a way that the light propagation direction in the fiber is parallel/perpendicular to the magnetic field direction. The resonant wavelength had a blueshift when the magnetic field angle was changed from 0° to 90° . After that, when the angle was changed from 90° to 180° , there was a redshift. The resonant wavelength was periodically changed as a function of the magnetic field angle as shown in Fig. 4(b). A linear fit of the experiment data for the angle range from 0° to 90° at random crystal orientation in Fig. 4(b) yields a magnetic field directional sensitivity of

0.132 pm/rad. Finally, the resonant wavelength response to the magnetic field angle is plotted in the polar coordinate system. There are symmetric “8-shaped” curves as shown in Fig. 4(c), indicating that the magnetic field directional sensitivity is not obviously influenced by the YIG crystal orientation.

4. Conclusion

In conclusion, A magnetic field sensor based on 500- μm -radius YIG microsphere cavities has been demonstrated. The measured magnetic sensitivity is 0.357 pm/mT, with a saturation threshold of 45 mT. Furthermore, the sensor can detect the direction of the magnetic field, achieving a maximum directional sensitivity of 0.132 pm/rad. Our all-optical on-chip magnetic sensor is attractive for weak magnetic vector signal detection at the millitesla level and has a compact footprint. Moreover, the sensor has good stability and repeatable performance showing a promising future for the distributed sensing scenarios in complex electromagnetic environments.

Funding. National Key Research and Development Program of China (SQ2023YFB2805600); Natural Science Foundation of Beijing Municipality (Z210004); National Natural Science Foundation of China (12474372, 62131002, 62101057, 62071448); State Key Laboratory of Information Photonics and Optical Communications (IPOC2021ZT01); Beijing Nova Program from Beijing Municipal Science and Technology Commission (20230484433); Fundamental Research Funds for the Central Universities (2024ZCJH14); Beijing University of Posts and Telecommunications Excellent Ph.D. Students Foundation (CX20241078).

Acknowledgments. The authors thank Dr. Xiao-Chong Yu for the helpful discussions. Author Bolun Zhang acknowledges funding from the Beijing Natural Science Foundation (Undergraduate Program) (QY24218).

Disclosures. The authors declare no conflicts of interest.

Data availability. Data underlying the results presented in this paper are not publicly available at this time but may be obtained from the authors upon reasonable request.

References

1. M. A. Khan, J. Sun, B. Li, *et al.*, “Magnetic sensors-A review and recent technologies,” *Eng. Res. Express* **3**(2), 022005 (2021).
2. A. Hojjati-Najafabadi, M. Mansoorianfar, T. Liang, *et al.*, “A review on magnetic sensors for monitoring of hazardous pollutants in water resource,” *Sci. Total Environ.* **824**, 153844 (2022).
3. L. Gloag, M. Mehdipour, D. Chen, *et al.*, “Advances in the application of magnetic nanoparticles for sensing,” *Adv. Mater.* **31**(48), 1904385 (2019).
4. D. Murzin, D. J. Mapps, K. Levada, *et al.*, “Ultrasensitive magnetic field sensors for biomedical applications,” *Sensors* **20**(6), 1569 (2020).
5. J. S. Bennett, B. E. Vyhalek, H. Greenall, *et al.*, “Precision magnetometers for aerospace applications: A review,” *Sensors* **21**(16), 5568 (2021).
6. H. Liu, H. Dong, J. Ge, *et al.*, “An overview of sensing platform-technological aspects for vector magnetic measurement: A case study of the application in different scenarios,” *Measurement* **187**, 110352 (2022).
7. Z. Yang, S. Pu, T. Xu, *et al.*, “Fiber-optic magnetic field sensor based on curved Terfenol-D rod combined with FBG,” *IEEE Sens. J.* **25**(4), 6234–6241 (2025).
8. Z. Hao, Y. Li, S. Pu, *et al.*, “Ultrahigh-performance vector magnetic field sensor with wedge-shaped fiber tip based on surface plasmon resonance and magnetic fluid,” *Nanophotonics* **11**(15), 3519–3528 (2022).
9. A. D. Charles, A. N. Rider, S. A. Brown, *et al.*, “Multifunctional magneto-polymer matrix composites for electromagnetic interference suppression, sensors and actuators,” *Prog. Mater. Sci.* **115**, 100705 (2021).
10. C. Liu, T. Shen, H. B. Wu, *et al.*, “Applications of magneto-strictive, magneto-optical, magnetic fluid materials in optical fiber current sensors and optical fiber magnetic field sensors: A review,” *Opt. Fiber Technol.* **65**, 102634 (2021).
11. B. Duan, H. Zou, J. H. Chen, *et al.*, “High-precision whispering gallery microsensors with ergodic spectra empowered by machine learning,” *Photonics Res.* **10**(10), 2343–2348 (2022).
12. Y. Wu, B. Duan, J. Song, *et al.*, “Simultaneous temperature and pressure sensing based on a single optical resonator,” *Opt. Express* **31**(12), 18851–18861 (2023).
13. D. Yu, M. Humar, K. Meserve, *et al.*, “Whispering-gallery-mode sensors for biological and physical sensing,” *Nat. Rev. Methods Primers* **1**(1), 83 (2021).
14. W. Liu, Y. L. Chen, S. J. Tang, *et al.*, “Nonlinear sensing with whispering-gallery mode microcavities: from label-free detection to spectral fingerprinting,” *Nano Lett.* **21**(4), 1566–1575 (2021).
15. X. Jiang, A. J. Qavi, S. H. Huang, *et al.*, “Whispering-gallery sensors,” *Matter* **3**(2), 371–392 (2020).
16. N. A. Toropov, M. C. Houghton, D. Yu, *et al.*, “Thermo-optoplasmonic single-molecule sensing on optical microcavities,” *ACS Nano* **18**(27), 17534–17546 (2024).

17. Y. Chen, Y. Yin, L. Ma, *et al.*, "Recent progress on optoplasmonic whispering-gallery-mode microcavities," *Adv. Opt. Mater.* **9**(12), 2100143 (2021).
18. M. C. Houghton, S. V. Kashanian, T. L. Derrien, *et al.*, "Whispering-gallery mode optoplasmonic microcavities: From advanced single-molecule sensors and microlasers to applications in synthetic biology," *ACS Photonics* **11**(3), 892–903 (2024).
19. H. Yang, X. Cao, Z. G. Hu, *et al.*, "Micropascal-sensitivity ultrasound sensors based on optical microcavities," *Photonics Res.* **11**(7), 1139–1147 (2023).
20. X. Ouyang, T. Liu, Y. Zhang, *et al.*, "Ultrasensitive optofluidic enzyme-linked immunosorbent assay by on-chip integrated polymer whispering-gallery-mode microlaser sensors," *Lab Chip* **20**(14), 2438–2446 (2020).
21. C. Yu, J. Janousek, E. Sheridan, *et al.*, "Optomechanical magnetometry with a macroscopic resonator," *Phys. Rev. Appl.* **5**(4), 044007 (2016).
22. B. B. Li, D. Bulla, V. Prakash, *et al.*, "Invited Article: Scalable high-sensitivity optomechanical magnetometers on a chip," *APL Photonics* **3**(12), 120806 (2018).
23. M. F. Colombano, G. Arregui, F. Bonell, *et al.*, "Ferromagnetic resonance assisted optomechanical magnetometer," *Phys. Rev. Lett.* **125**(14), 147201 (2020).
24. S. Vincent, X. Jiang, P. Russell, *et al.*, "Thermally tunable whispering-gallery mode cavities for magneto-optics," *Appl. Phys. Lett.* **116**(16), 161110 (2020).
25. C. Z. Chai, Z. Shen, Y. L. Zhang, *et al.*, "Single-sideband microwave-to-optical conversion in high-Q ferrimagnetic microspheres," *Photonics Res.* **10**(3), 820–827 (2022).
26. G. T. Xu, M. Zhang, Y. Wang, *et al.*, "Magnonic frequency comb in the magnomechanical resonator," *Phys. Rev. Lett.* **131**(24), 243601 (2023).
27. W. Liu, W. Li, R. Wang, *et al.*, "Magnetic sensor based on WGM hollow microbubble resonator filled with magnetic fluid," *Opt. Commun.* **497**, 127148 (2021).
28. C. Q. Yu, R. Niu, Z. D. Peng, *et al.*, "A current sensor based on capillary microresonator filled with Terfenol-D nanoparticles," *IEEE Photonics Technol. Lett.* **33**(5), 239–242 (2021).
29. C. Yu, S. Ma, H. Ren, *et al.*, "AC field modulated DC magnetic field sensor based on optical whispering gallery mode microcapillary resonator," *Opt. Express* **30**(13), 24062–24071 (2022).
30. Y. N. Zhang, N. Zhu, P. Gao, *et al.*, "Magnetic field sensor based on ring WGM resonator infiltrated with magnetic fluid," *J. Magn. Magn. Mater.* **493**, 165701 (2020).
31. G. T. Xu, Z. Shen, Y. Wang, *et al.*, "Optomechanical magnetometry on a bubble resonator with YIG microsphere," *IEEE Photonics Technol. Lett.* **35**(7), 393–396 (2023).
32. C. Yu, Y. Hu, K. Chen, *et al.*, "Alternative magnetic field sensor based on modified yttrium iron garnet (YIG) microspheres and a magnetostrictive material," *Instrum. Sci. Technol.*, 1–11 (2025).
33. P. Wang, M. Zhu, F. Pang, *et al.*, "Cylindrical vector beams for alternating magnetic field sensing based on YIG crystal," *IEEE Photonics Technol. Lett.* **35**(19), 1031–1034 (2023).
34. A. Prabhakar and D. D. Stancil, *Spin Waves: Theory and Applications* (Springer, 2009).
35. Z. Hao, S. Pu, J. Wang, *et al.*, "Dual-channel temperature-compensated vector magnetic field sensor based on lab-on-a-fiber-tip," *Opt. Express* **30**(14), 25208–25218 (2022).